Ab initio calculations of ferroelectric instability in $PbTiO_3$ capacitors with symmetric and asymmetric electrode layers

Yoshitaka Umeno,[1,2] Jan Michael Albina,[3] Bernd Meyer,[4] and Christian Elsässer[3,2]
[1]*Institute of Industrial Science, The University of Tokyo, 4-6-1 Komaba, Meguro-ku, Tokyo 153-8505, Japan*
[2]*IZBS, University of Karlsruhe, Kaiserstr. 12, 76131 Karlsruhe, Germany*
[3]*Fraunhofer Institute for Mechanics of Materials IWM, Wöhlerstr. 11, 79108 Freiburg, Germany*
[4]*Interdisciplinary Center for Molecular Materials (ICMM) and Computer-Chemistry-Center (CCC), University of Erlangen-Nürnberg, Nägelsbachstr. 25, 91052 Erlangen, Germany*
(Received 12 August 2009; revised manuscript received 23 October 2009; published 30 November 2009)

To investigate the influence of symmetric and asymmetric electrode layers on ferroelectric properties of perovskite capacitors, *ab initio* calculations based on density-functional theory using the local density approximation and the mixed-basis pseudopotential method are performed for $Pt/PbTiO_3/Pt$, $Pt/PbTiO_3/SrRuO_3$, and $SrRuO_3/PbTiO_3/SrRuO_3$ models. $SrRuO_3/PbTiO_3/SrRuO_3$ capacitors with PbO-terminated $PbTiO_3$ layers have a ferroelectric stability similar to that of $Pt/PbTiO_3/Pt$, while the ferroelectricity is strongly suppressed in the capacitors with TiO_2-termination. The asymmetric combination of the electrodes enhances the ferroelectric polarization pointing from $SrRuO_3$ to Pt while the opposite polarization becomes less stable. The epitaxial lattice strain does not strongly affect the electronic Schottky barriers of the symmetric capacitors. The contribution of the electrical field originating from the asymmetric electrodes influences the Schottky barriers significantly. The switching of the polarization in the asymmetric capacitor changes the Schottky barrier height from $PbTiO_3$ to the $SrRuO_3$ electrode by about 1.0 eV.

DOI: 10.1103/PhysRevB.80.205122 PACS number(s): 77.80.−e, 77.84.Dy, 77.22.Ej, 31.15.A−

I. INTRODUCTION

Nonvolatile data storage is a key challenge for advancing the development of information technology. The ferroelectric random access memory (FeRAM), which utilizes the hysteresis of spontaneous electrical polarization (ferroelectricity), is promising for a substantial improvement of nonvolatile memory devices since the polarization switching occurs within 1 ns, which enables swift function as DRAM (dynamic random access memory). The FeRAM has advantages over the widely used EEPROM (electrically erasable programmable read only memory, namely, the flash memory) in terms of fast read/write operation and electric efficiency. As FeRAM devices encountered mass production and were put on the market a few years ago, further development of its efficiency and reliability are likely to be accelerated. It is essential, therefore, to elucidate the functional properties of FeRAMs (ferroelectric and electronic).

Finding the minimum thickness for ferroelectricity in a perovskite thin-film capacitor is an important issue owing to the growing demand on designing smaller devices for advanced efficiency and performance. Theoretical *ab initio* studies by means of density-functional theory (DFT) have contributed to this issue, and the ferroelectricity of ultrathin perovskite films, which are typical ferroelectric materials sandwiched with electrode layers, has been investigated. The first *ab initio* study was carried out by Junquera *et al.*[1] to find that $BaTiO_3$ thin films between two $SrRuO_3$ electrodes lose the ferroelectric properties below a critical thickness of about 24 Å. Subsequent *ab initio* studies have revealed that the critical thickness depends on the electrode material as well as on the termination of the perovskite layer, indicating a strong influence of the chemical nature of perovskite-electrode interfaces.[2,3] In our previous study,[3] it was also demonstrated that the ferroelectric stability of $Pt/PbTiO_3/Pt$ capacitors depends on the epitaxial strain, i.e., the in-plane lattice constant; the ferroelectric state becomes more stable with decreasing lattice parameters.

While the ferroelectric properties of ultra-thin perovskite capacitors have so far been investigated theoretically only with identical electrode layers on both sides, in most experiments until now dissimilar materials are usually used for the bottom and top electrodes because different properties are required for the two electrodes. Metals resistant against oxidation, such as Pt, are suitable for the top electrode as it covers and protects the capacitor in gaseous environments. The bottom layers must have good epitaxial growth properties, and namely, the perovskite $SrRuO_3$ (SRO) is best suited, because of its close structural relationship and lattice match to the ferroelectric perovskites $PbTiO_3$ and $BaTiO_3$ and to typically used substrates [e.g., $SrTiO_3$ (STO)], enabling epitaxy on a perovskite substrate with well-ordered atomic arrangement. It is therefore of importance to investigate the ferroelectric properties of capacitors with different electrodes and to examine the effect of the asymmetry. Asymmetrical interface terminations of ferroelectric perovskite films were considered by Duan *et al.*,[4] Stengel *et al.*,[5] and Gerra *et al.*[6] Nevertheless, to our knowledge, no theoretical study has been reported which investigates the effect of the asymmetry of electrodes on the ferroelectricity in ultra-thin perovskite capacitors.

In this study, we perform *ab initio* DFT calculations of capacitors of $PbTiO_3$ (PTO) films between electrodes. We examine both symmetric (SRO/PTO/SRO) and asymmetric (Pt/PTO/SRO) capacitors to investigate influence of the electrodes on the ferroelectric stability. The results are also compared with those for Pt/PTO/Pt capacitors obtained in our previous study.[3]

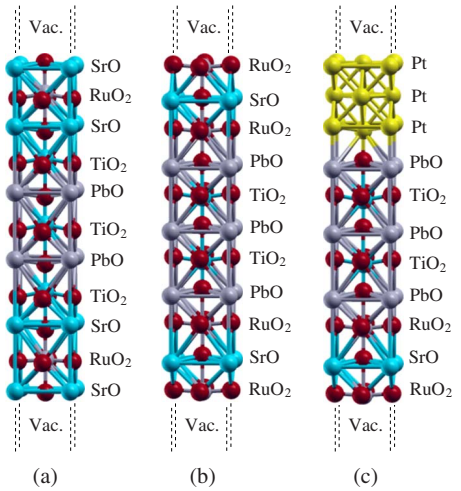

FIG. 1. (Color online) Simulation supercells for $m=2$. (a) and (b): Symmetric $SrRuO_3/PbTiO_3/SrRuO_3$ capacitors with the two possible terminations of $PbTiO_3$. (c): Asymmetric $Pt/PbTiO_3/SrRuO_3$ capacitor with PbO-terminated $PbTiO_3$.

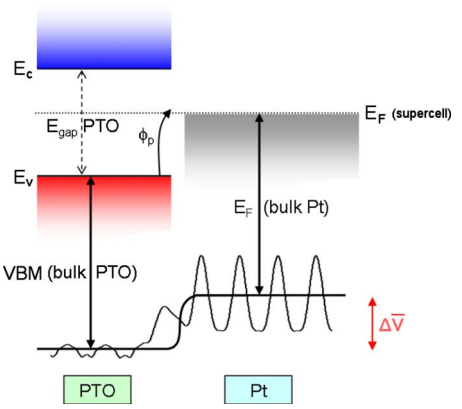

FIG. 2. (Color online) Principle of the *p*-type Schottky barrier height calculation for a PTO/Pt heterophase system with the difference $\Delta\bar{V}$ between the macroscopic average of the electrostatic potential. E_F and VBM are the Fermi energy and the valence-band maximum of the bulk material calculated independently. E_c and E_v, are the conduction-band edge and valence-band edge in the supercell, respectively.

II. COMPUTATIONAL DETAILS

The computations were performed using the mixed-basis pseudopotential (MBPP) code[7,8] employing norm-conserving pseudopotentials[9] and a mixed-basis set[10–12] of plane waves (with a cutoff energy of 20 Ry=272 eV) and localized basis functions (for more details see Refs. 13–15). The Brillouin-zone integrations were carried out with a $6\times6\times1$ Monkhorst-Pack[16] *k*-point mesh together with a 0.2 eV Gaussian broadening.[17]

We used a similar setup of simulation models as in our previous study,[3] where the validity of the pseudopotential approach was also examined by the comparison with ultrasoft pseudopotentials[18] and the projector augmented wave method[19] implemented in the Vienna *ab Initio* simulation package.[20,21] The ultrathin (001)-oriented PTO films between electrodes were represented by electrode-perovskite-electrode multilayer models as shown in Fig. 1. We examined both symmetric (SRO/PTO/SRO) and asymmetric (Pt/PTO/SRO) capacitors. To investigate the two possible terminations of the perovskite (001) surface, PbO and TiO_2, the following model setups were made: RuO_2-SrO-RuO_2/PbO-$(TiO_2$-PbO$)_m$/RuO_2-SrO-RuO_2 and SrO$-RuO_2-$SrO$/TiO_2-$(PbO$-TiO_2)_m$/SrO-RuO_2-SrO for symmetric capacitors, and Pt_3/PbO-$(TiO_2-$PbO$)_m$/RuO_2-SrO-RuO_2 for an asymmetric one, where *m* denotes the number of perovskite unit cells in the PTO film.

A vacuum region is included in our supercell models separating the metal electrodes on the two sides of the perovskite films to enable the calculation of the asymmetric capacitor. This setup gives the electrical short-circuit condition as well as an electrode/perovskite superlattice geometry.[22]

The configurations of paraelectric (PE) and ferroelectric (FE) phases were obtained by structural relaxation with and without imposed centrosymmetry, respectively. The relaxation was performed with a predetermined lateral lattice parameter, *a*, until the maximum force on the atoms was less than 0.01 eV/Å. The relaxed energies were obtained as a function of *a*. For the symmetric capacitors, the ferroelectric stability was evaluated by the energy difference between the paraelectric and ferroelectric phases. On the other hand, the paraelectric phase configuration cannot be well defined for the asymmetric capacitors. Therefore, we took the average of the PE energies of the two symmetric capacitors (Pt/PTO/Pt and SRO/PTO/SRO) with the same perovskite thickness for a paraelectric zero-energy reference energy, i.e.,

$$E^{\mathrm{PPS}}(\mathrm{PE}) \equiv \frac{E^{\mathrm{PPP}}(\mathrm{PE}) + E^{\mathrm{SPS}}(\mathrm{PE})}{2}, \tag{1}$$

where PPS, PPP, and SPS refer to Pt/PTO/SRO, Pt/PTO/Pt, and SRO/PTO/SRO, respectively.

In order to investigate the influence of the electrode materials on the electronic properties of the capacitors, we calculated the Schottky barrier heights for holes and electrons using a macroscopic averaging of the electrostatic potential.[14,15,23–25]

As shown in Fig. 2, the *p*-type Schottky barrier is calculated as

$$\phi_p = \Delta\bar{V} + \Delta E_{\mathrm{bulk}}, \tag{2}$$

with the difference $\Delta\bar{V}$ between the macroscopic averages of the electrostatic potentials in the two materials far from the interface and the difference ΔE_{bulk} between the Fermi energy of the electrode and the valence-band maximum (VBM) of the dielectric material. The Fermi energies and VBM are obtained from independent bulk calculations using the same strain conditions as in the capacitor supercell calculations.

III. RESULTS AND DISCUSSION

A. Ferroelectric instability of the capacitors

For symmetrical SRO/PTO/SRO capacitors [see Figs. 1(a) and 1(b)], Fig. 3 shows the energy difference of the FE and

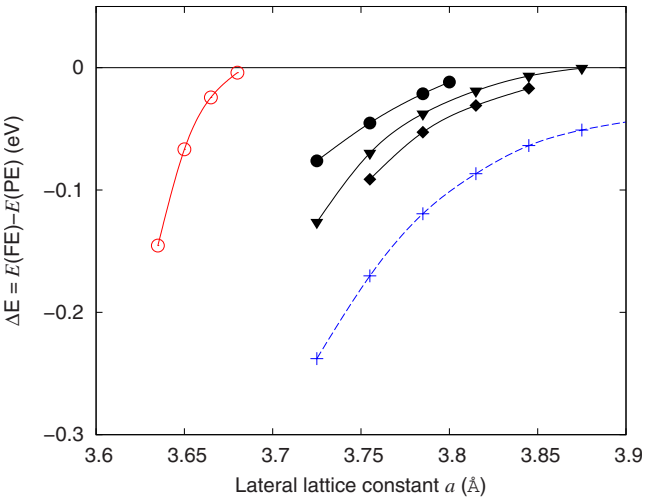

FIG. 3. (Color online) Ferroelectric stability of $SrRuO_3/PbTiO_3/SrRuO_3$ capacitors. Energy difference ΔE per $PbTiO_3$ perovskite unit cell between the FE and PE state as a function of the in-plane lattice constant a. Open and closed symbols are for TiO_2- and PbO-terminated films, respectively (circles, $m=2$; triangles, $m=4$; diamonds, $m=6$; pluses, $m=\infty$, i.e., bulk $PbTiO_3$, cf. Ref. 3).

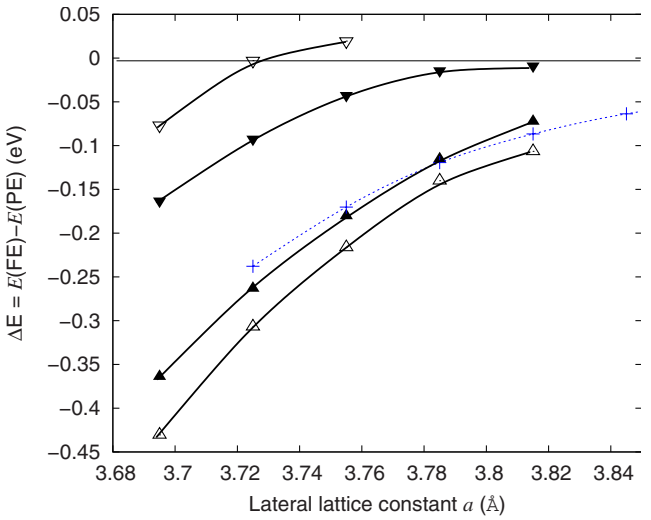

FIG. 4. (Color online) Ferroelectric stability ΔE of $Pt/PbTiO_3/SrRuO_3$ capacitors with PbO-terminated perovskite layers. Open and closed symbols are for $m=2$ and 4, respectively. Up-triangles and down-triangles denote polarizations of the opposite directions. The bulk result ($m=\infty$) is also shown for comparison (pluses).

PE states, $\Delta E=[E(\mathrm{FE})-E(\mathrm{PE})]/m$, which presents the ferroelectric stability: the more negative value means the more stable FE state. As in the case of Pt/PTO/Pt capacitors in our previous study,[3] ΔE depends on the lateral lattice parameter and the FE state becomes more stable as the lattice parameter decreases. The FE stability is again clearly dependent on the interface termination. The FE polarization requires a much smaller lateral lattice parameter a in a capacitor with TiO_2-terminated PTO layers than in that with PbO termination. The critical lateral lattice constant for ferroelectricity in a $m=2(\sim 16$ Å) capacitor is 3.82 Å and 3.68 Å for PbO and TiO_2 terminations, respectively, which are estimated by extrapolation of the $m=2$ curves. While the former value is close to that of Pt/PTO/Pt, the latter is much smaller (see Fig. 2 in Ref. 3). This indicates that the TiO_2-termination of PTO layers at the SRO/PTO interface strongly suppresses the ferroelectric polarization perpendicular to the interface.

The ferroelectric stability of the asymmetric Pt/PTO/SRO capacitor is shown in Fig. 4. Because of the asymmetry in the structure, the FE states with opposite polarization directions exhibit different energies relative to the PE reference state. The relaxed FE configurations of the $m=2$ capacitors at $a=3.725$ Å are shown in Fig. 5. The "FE1" structure, where the oxygen atoms shift toward the Pt layer and metal atoms Ti and Pb toward SRO (i.e., resulting in a negatively charged Pt side and positive SRO), exhibits the lower FE stability (triangles down in Fig. 4). The FE stability decreases (ΔE increases) with increasing lateral lattice parameter, and the FE1 state is no longer stable at $a\geq 3.785$ Å in the $m=2$ capacitors: when the relaxed FE1 structure at $a=3.755$ Å was stretched in the in-plane directions to have $a=3.785$ Å and then relaxed, the polarization direction flipped to the FE2 structure. On the other hand, the FE2 states have an even higher FE stability than the bulk crystal. This indicates that the asymmetric combination of electrode layers enhances the spontaneous polarization in the direction of FE2. It is interesting to note that both of the electrode/perovskite interfaces, Pt/PTO and SRO/PTO, suppress the ferroelectric polarization in the symmetric thin-film structure.

In our previous work[3] we showed that the ferroelectric stability of a Pt/PTO/Pt capacitor of $m\geq 4$ can be estimated by extrapolation using ΔE data for $m=2$ and $m=\infty$. Here we examine the same extrapolation for SRO/PTO/SRO. The FE stability for $m=4$ is estimated by the extrapolation

$$\Delta E_{\mathrm{ext}}(m=4)=[2\Delta E(m=2)+2\Delta E(m=\infty)]/4, \qquad (3)$$

where the subscript "*ext*" denotes the extrapolated value, which is shown in Fig. 6 with a dashed line. The extrapolated line deviates from the calculated ΔE, indicating that the extrapolation scheme does not work for $m=4$. This means that the SRO/PTO interface influences not only the FE displacement in one outermost PTO unit cell but also that in the center cells. Assuming that the influence is limited to the two outer unit cells from the interfaces (i.e., four cells in total), ΔE for $m=6$ can be estimated by

$$\Delta E_{\mathrm{ext}}(m=6)=[4\Delta E(m=4)+2\Delta E(m=\infty)]/6, \qquad (4)$$

which is shown by a dotted-dashed line in the figure. The discrepancy seen in Fig. 6 between the extrapolation and the calculated FE stability for $m=6$ demonstrates the invalidity of the simple assumption. Hence, unlike the Pt/PTO interface, the influence of the SRO/PTO interface is longer ranged. However, the discrepancy for $m=6$ is much smaller than for $m=4$, implying that the extrapolation scheme eventually will work for thicker slabs.

While $m=4$ is sufficient for both the PbO-terminated Pt/PTO/Pt and SRO/PTO/SRO capacitors to have stable ferroelectric states at $a=3.845$ Å (the *ab initio* calculated cubic lattice parameter of the typical substrate material STO, cf.

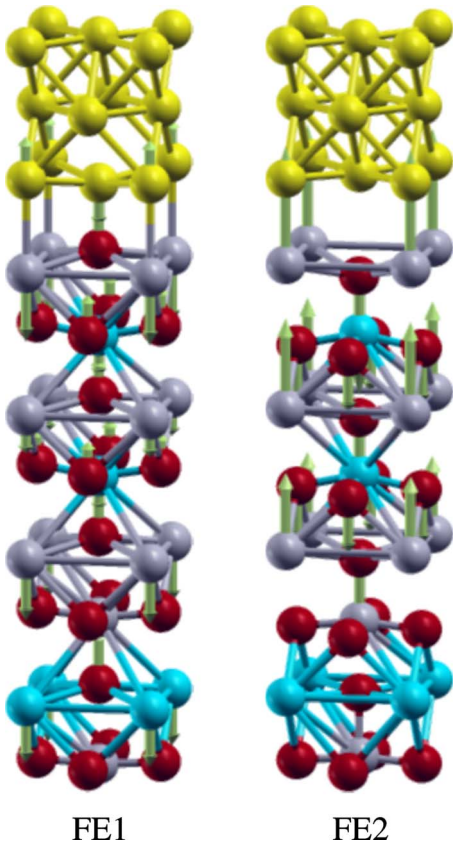

FIG. 5. (Color online) Atomic configurations of the two FE polarizations of the $m=2\mathrm{Pt}/\mathrm{PbTiO_3}/\mathrm{SrRuO_3}$ capacitor at $a=3.725$ Å. Arrows indicate the FE shift of atoms (length is multiplied for visibility) from the averaged coordinate of each TiO_2 or PbO atomic layer.

Refs. 3 and 13) thicker layers are expected to be necessary for the Pt/PTO/SRO one. I.e., the ferroelectric state in the asymmetric capacitors becomes unstable already at smaller lattice parameters than in the symmetric ones. This is because the ferroelectric state with the polarization pointing to the SRO side (FE1) is suppressed by the combination of the dissimilar electrodes, while the polarization in the opposite direction (FE2) is stabilized. It is reasonable to expect that the curves of the ferroelectric stability asymptotically become closer to that of bulk PTO as the thickness of the PTO layers increases, while FE1 remains less stable than FE2. The stability of the FE1 state, therefore, presumably determines whether the capacitor is ferroelectric or not.

The ferroelectric stability of the Pt/PTO/SRO capacitor is discussed in this paper in terms of energy differences between the ferroelectric state and the zero-energy reference energy [Eq. (1)]. This scheme is valid because, as seen in Fig. 4, the energy of the FE1 state asymptotically comes close to the reference energy with an increasing lattice parameter until the polarization direction is reversed. To estimate accurately the ferroelectric stability of the asymmetric capacitor, one needs to calculate the activation energy required to switch one ferroelectric state to the other by a more sophisticated scheme, such as the nudged elastic band (NEB) approach,[26] to obtain the energy at the transition barrier

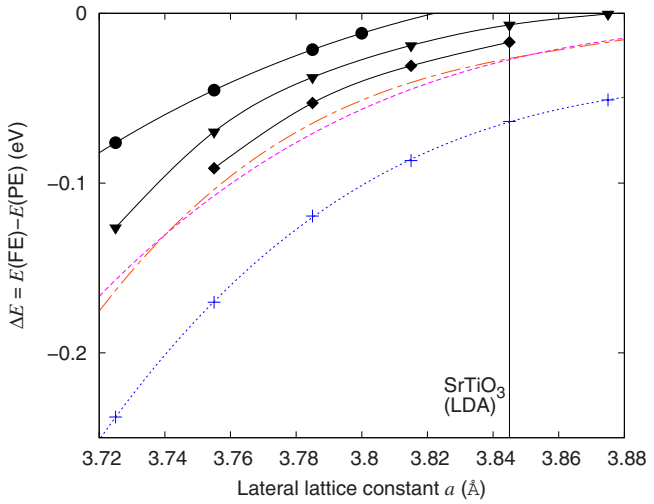

FIG. 6. (Color online) Ferroelectric stability ΔE per $PbTiO_3$ unit cell of the PbO-terminated $\mathrm{SrRuO_3}/\mathrm{PbTiO_3}/\mathrm{SrRuO_3}$ capacitor. Symbols are the same as in Fig. 3. The dashed and dotted-dashed lines are extrapolations for $m=4$ and 6, respectively, according to Eqs. (3) and (4).

(saddle point) in the energy landscape between the two ferroelectric states polarized in the opposite directions. This computation is, however, rather expensive and we consider it beyond the scope of this paper.

The analysis of the local densities of states for oxygen revealed the presence of numerous induced gap states in the PbO layer at the interface for the PbO-terminated film. For the TiO_2-terminated film almost no gap states were observed in the TiO_2 layer at the interface. One reason for the suppression of ferroelectricity in the TiO_2-terminated film is likely the presence of an insulating interfacial TiO_2-SrO layer (effectively an STO unit) between PTO and SRO in this case.

B. Analysis of atomic displacements

In this section the atomic displacements, in terms of layer rumplings, related to the ferroelectric states as function of lateral strain and film thickness are analyzed. The layer rumpling, η, in PTO and SRO is defined for each atomic plane, i, as $\eta_i=[\bar{\delta}_z(\mathrm{M}_i)-\bar{\delta}_z(\mathrm{O}_i)]$, where $\bar{\delta}_z(\mathrm{M}_i)$ and $\bar{\delta}_z(\mathrm{O}_i)$ denote the averaged displacements of metal and oxygen atoms normal to the atomic plane, respectively. For the Pt layers, η is defined by $\eta_i=[\delta_z(\mathrm{Pt}_i^{\mathrm{cnt}})-\delta_z(\mathrm{Pt}_i^{\mathrm{cor}})]$, where $\mathrm{Pt}^{\mathrm{cnt}}$ and $\mathrm{Pt}^{\mathrm{cor}}$ denote Pt atoms in the center and on the corner of the (001) unit cell, respectively. Layer rumplings in the asymmetric capacitors with varying lattice parameters are plotted in Fig. 7. It is seen that the rumplings in the Pt and SRO layers are large for the FE1 polarization while those in FE2 are moderate, which indicates the larger distortion in the electrode layers that results in the lower ferroelectric stability of FE1. The magnitude of rumplings in the PTO layers decreases with increasing lattice parameters, corresponding to the reduction in the ferroelectric stability as a function of a. At the small lattice parameters, the rumplings of PbO layers are larger than those of TiO_2, as evident from the zigzag lines of the layer rumpling. The lines become more flat at larger a.

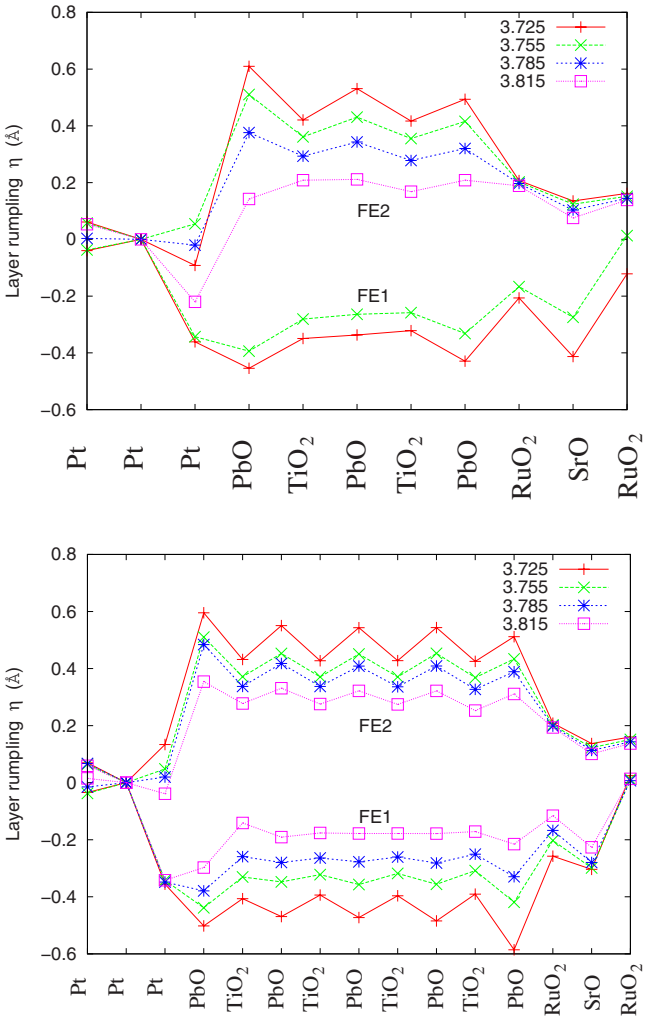

FIG. 7. (Color online) Atomic layer rumpling in the relaxed $Pt/PbTiO_3/SrRuO_3$ capacitor. (a) $m=2$ and (b) $m=4$.

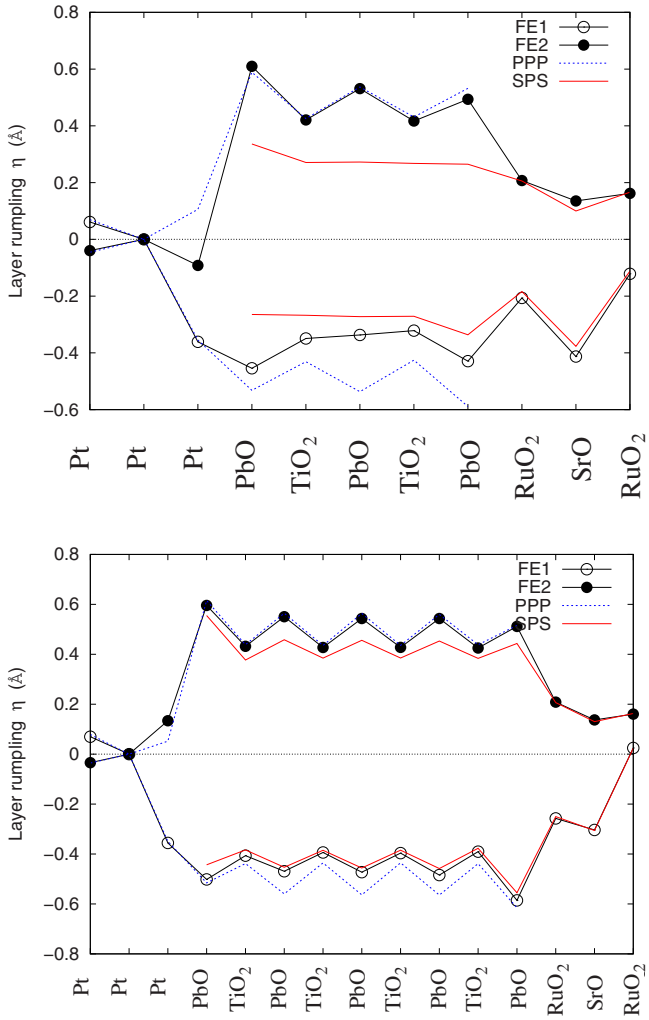

FIG. 8. (Color online) Atomic layer rumpling in the relaxed $Pt/PbTiO_3/SrRuO_3$ capacitor at $a=3.725$ Å. (a) $m=2$ and (b) $m=4$.

The layer rumplings in the Pt/PTO/SRO capacitors with $a=3.725$ Å are compared with those in Pt/PTO/Pt and SRO/PTO/SRO in Fig. 8. For $m=2$, the rumplings in the PTO layers with FE2 polarization are close to those in Pt/PTO/Pt, while the PTO rumplings of FE1 are affected by the PTO/SRO interface. This indicates that the influence of the PTO/SRO interface on the polarization of the PTO layers depends on the polarization direction, which explains the difference of ferroelectric stability between the FE1 and FE2 states. For $m=4$, the rumplings of the PTO layers in the Pt/PTO/SRO capacitor are closer to those in the symmetric ones, but they are still slightly suppressed in the FE1 state. It is expected that even thicker layers are required for the center cells to have a polarization close to that of bulk PTO.

C. Analysis of electrostatic potentials and Schottky barriers

In the following we analyzed the electronic properties of the Pt/PTO/Pt, SRO/PTO/SRO, and Pt/PTO/SRO heterostructures. In order to ensure an accurate determination of the electrode potential level, we introduced two additional layers in both, the Pt and SRO electrodes. The interlayer spacing of the additional layers was determined by calculating the minimum energy configuration of strained unit cells of Pt and SRO with the lateral lattice parameter fixed to $a=3.845$ Å of an STO substrate. No further relaxation steps were carried out since the resulting structure was found to be already a good approximation of the final relaxed structure. As an example, the SRO/PTO/SRO PE capacitor with TiO_2 terminated PTO and five layer electrode was fully relaxed. The difference in potential levels was found to be less than 0.04 eV. Figure 9 shows the influence of the increasing number of electrode layers on the averaged electrostatic potentials for the Pt/PTO/Pt and the SRO/PTO/SRO heterostructures in the PE state with $a=3.845$ Å. It is interesting to note how the averaged potential of the electrode slab is converging to a constant level with the addition of supplementary layers. We chose to employ electrode slabs containing five layers as it was found to provide a large enough layer thickness for an accurate determination of the potential levels (cf. Refs. 14 and 15).

We focused our investigation of the electronic properties on heterophase systems with the two lattice parameters $a=3.815$ Å and $a=3.845$ Å where the system are not stable

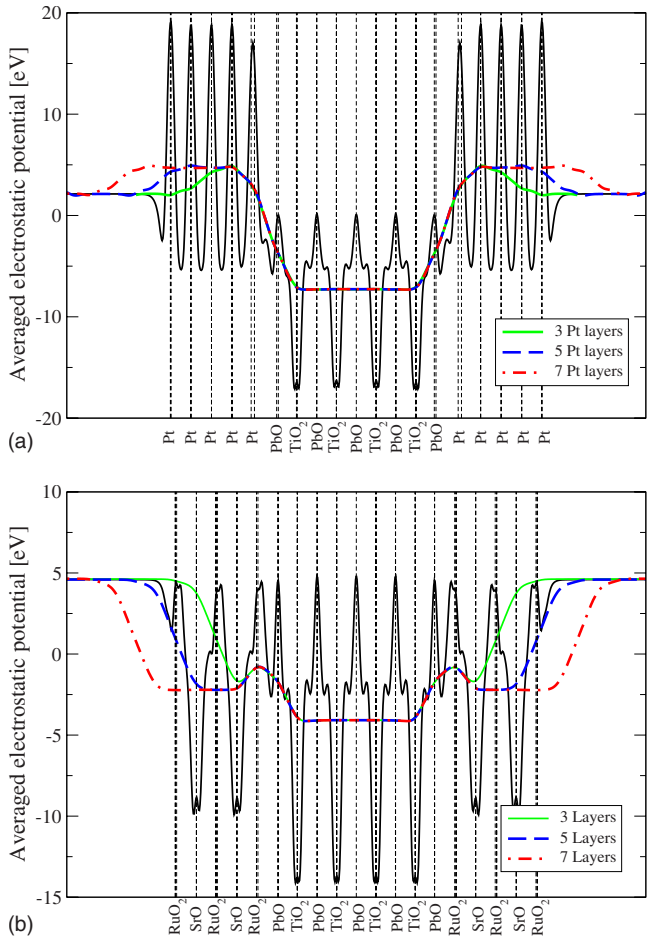

FIG. 9. (Color online) Planar average (continuous black line) and macroscopic averages (colored lines) of the electrostatic potential in (a) the Pt/PTO/Pt and (b) the SRO/PTO/SRO capacitors for the PE state and various thicknesses of the electrode layers. For clarity we show only the planar average for an electrode of five layers. The lattice parameter is a=3.845 Å of STO. The dashed vertical lines mark positions of atom planes.

in FE and PE states, respectively. In a first step, the Schottky barriers were evaluated by measuring the potential level located in the most central part of the PTO slab, i.e., we omitted the effect of FE polarization on the barriers. For the smaller lattice parameter (a=3.815 Å), the Schottky barriers were analyzed for the Pt/PTO/Pt (FE), SRO/PTO/SRO (FE), and the Pt/PTO/SRO (FE1 and FE2) capacitors. The larger lattice parameter (a=3.845 Å) was used to calculate the Schottky barriers of the PE systems, namely, the Pt/PTO/Pt and SRO/PTO/SRO capacitors with PbO and TiO_2 terminations. For comparison, we included the PbO-terminated Pt/PTO/Pt and SRO/PTO/SRO capacitors with FE state. The computed Schottky barrier values are listed in Table I. We use the convention of positive offset for an upward step when going from the left (Pt or SRO) to the right slab (PTO). The same convention is used for the asymmetric electrodes capacitors where the second value is for a step from the PTO (now left slab) to the Pt or SRO (right slab). The Schottky barriers for electrons are estimated by using the experimental bandgap of PTO, $E_{\mathrm{gap}}^{\mathrm{PTO}}$=3.778 eV,[27] so that $|\phi_n|=E_{\mathrm{gap}}^{\mathrm{PTO}}-|\phi_p|$.

By using the most central part of the PTO slab, we are reporting in the Table I an average value of the Schottky barriers. Evaluating the contribution of the electrical field on the barrier heights is challenging since one has to consider the electrical field arising from the spontaneous polarization of PTO and from the external electrical field due to the asymmetrical electrodes in Pt/PTO/SRO capacitors. However, in the following we attempted to estimate the Schottky barriers values in the presence of the inherent electrical field. The corresponding barriers, presented in the Table I in italic, were evaluated at the intersection of the nanosmoothed potential line for PTO with its most external layer position. The results obtained by this method should be considered only as indicative since the position of the interface is arbitrarily chosen. Also informative is the relative polarity (RP) that we define as the ratio of the maximum potential level for a selected capacitor with respect to the potential level of a reference capacitor. This parameter has the advantage to be independent of the location of the interface. It can be regarded as an indicator of the strength of the field in the PTO slab since the slope of the macroscopically averaged electrostatic potential in PTO from different capacitors is compared. The potential level of the Pt/PTO/Pt FE system was chosen as a reference, i.e., it is RP=1.0.

As a general remark, the Schottky barrier for electrons is always larger by a factor of 1.5 to 3 than the Schottky barrier for holes (cf. Refs. 14 and 15). Concerning the averaged Schottky barriers, i.e., without taking into account the electrical field, the values for the Pt/PTO/Pt FE capacitor are not significantly modified by the increase in lattice parameter ($\Delta\phi$=0.06 eV when a changes from 3.815 Å to 3.845 Å). The paraelectric state is slightly increasing (decreasing) the Schottky barrier for holes (electrons) with respect to the ferroelectric state. However, their differences are not much larger than the computational uncertainty of about 0.1 to 0.2 eV usually obtained for this method.[14,15,28,29] The termination of the PTO slab is not changing considerably the Schottky barriers of the PE state, with 1.27 and 1.54 eV for the PbO and TiO_2 termination, respectively. As for the SRO/PTO/SRO FE capacitor, the change in the lattice parameter does not affect strongly the Schottky barriers taking into account the numerical uncertainty of $0.1 \sim 0.2$ eV. However, the barrier difference between the PE and the FE state is larger than in the Pt/PTO/Pt system with an amount of 0.35 eV. Moreover, a larger difference is observed for the TiO_2 terminated PTO slab, with a smaller (larger) Schottky barrier for holes (electrons) than for the PbO-terminated PTO slab. This emphasizes the role of bonding mechanisms at the interface for oxidic vs. metallic electrode materials. While we obtain a Schottky barrier for holes of 1.04 eV for the Pt/PTO/Pt FE and 1.29 eV for the SRO/PTO/SRO FE systems, the Pt/PTO/SRO FE1 capacitor has a similar value 1.35 eV for the SRO electrode side but a larger value with 1.32 eV for the Pt electrode side. On the contrary, the Pt/PTO/SRO FE2 capacitor shows a reduction in the Schottky barriers for holes with 0.90 eV for the Pt electrode side and 0.87 eV for the SRO electrode side. This indicates that the contribution of the electrical field generated in the case of asymmetric electrodes is influencing the Schottky barriers.

Concerning the Schottky barriers by taking into account the electrical fields, the RP shows a three times higher inter-

TABLE I. Schottky barriers for holes ϕ_p and for electrons ϕ_n for the Pt/PTO/Pt, SRO/PTO/SRO, and the Pt/PTO/SRO capacitors with two lateral lattice parameters a=3.815 Å and a=3.845 Å. The numbers in italic correspond to the modified Schottky barriers by taking into account the effect of the electrical field. RP is the relative polarity (see text). All PTO slabs are PbO terminated except for the capacitors of the last two lines which are TiO_2 terminated [marked with (*)].

	ϕ_p (eV)	ϕ_n (eV)	RP
		a=3.815 Å	
Pt/PTO/Pt—FE	−1.04	2.74	
	−1.04 ± 0.10	2.74 ± 0.10	*1.0*
Pt/PTO/SRO—FE1	−1.32 (Pt) 1.35 (SRO)	2.46 (Pt) −2.43 (SRO)	
	−1.05 *(Pt)* *1.61 (SRO)*	*2.73 (Pt)* −2.17 *(SRO)*	*2.7 (Pt) 2.9 (SRO)*
Pt/PTO/SRO—FE2	−0.90 (Pt) 0.87 (SRO)	2.88 (Pt) −2.91 (SRO)	
	−1.03 *(Pt)* *0.74 (SRO)*	*2.75 (Pt)* −3.04 *(SRO)*	*−1.3 (Pt) −1.3 (SRO)*
SRO/PTO/SRO—FE	−1.29	2.49	
	−1.29 ± 0.30	2.49 ± 0.30	*3.0*
		a=3.845 Å	
Pt/PTO/Pt—FE	−1.10	2.68	
	−1.10 ± 0.10	2.68 ± 0.10	*1.0*
Pt/PTO/Pt—PE	−1.27	2.51	
SRO/PTO/SRO—FE	−1.22	2.56	
	−1.22 ± 0.29	2.56 ± 0.29	*2.9*
SRO/PTO/SRO—PE	−1.57	2.21	
Pt/PTO/Pt—PE*	−1.54	2.24	
SRO/PTO/SRO—PE*	−0.91	2.87	

nal field in PTO when SRO electrodes are used instead of Pt electrodes. This is independent of the lattice parameter. The Pt/PTO/SRO FE1 asymmetric capacitor has RP≃2.8 which is comparable to the symmetric SRO/PTO/SRO FE capacitor. The Pt/PTO/SRO FE2 capacitor exhibits a field that is much lower (with RP=1.3 similar to the symmetric Pt/PTO/Pt FE capacitor) than in the FE1. The difference in potential levels between Pt and SRO creates a field going from the Pt toward the SRO. Therefore, the Pt/PTO/SRO FE2 which can be regarded as a Pt/PTO/SRO FE1 capacitor with inverse electrodes is subject to a field that is opposing the polarization of PTO, resulting in a smaller internal field in the PTO slab. The somewhat larger rumpling of the atomic layers observed in FE2 is suggesting that larger surface polarization are occurring, as pointed out by Meyer and Vanderbilt[30] for a free PTO surface slab under negatively oriented external electrical fields.

It is interesting to note that the Schottky barrier values for Pt are rather uniform with ϕ_p=1.0–1.1 eV and ϕ_n=2.7–2.8 eV. This may indicate that the Schottky barrier between Pt/PTO is rather insensitive to the polarization state of PTO. This is not the case for SRO where the barriers vary significantly and "follow" the polarization field with, e.g., ϕ_n decreasing from 2.49 to 2.17 eV in the case of FE1 and increasing up to 3.04 eV for FE2. This suggests that switching the polarization state of PTO in a Pt/PTO/SRO capacitor will increase or decrease the Schottky barrier of the SRO electrode with a magnitude of almost 1.0 eV, as schematically represented in Fig. 10.

IV. CONCLUSION

To reveal the role of asymmetric and symmetric bottom and top electrodes in ferroelectric perovskite capacitors, we performed *ab initio* DFT calculations of Pt/PTO/SRO and SRO/PTO/SRO multilayer models. Schottky barriers were analyzed not only for these two models but also the Pt/PTO/Pt model investigated in our previous study.[3]

Similarly to Pt/PTO/Pt capacitors, a strong dependence of the ferroelectric stability on the lateral lattice parameter was found both in SRO/PTO/SRO and Pt/PTO/SRO capacitors:

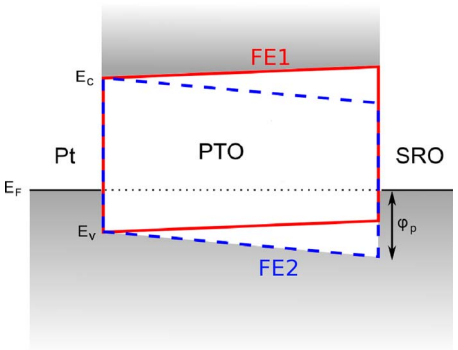

FIG. 10. (Color online) Variation in the Schottky barrier height by switching of the FE polarization in PTO. While the barrier height is rather constant for the Pt electrode, the barrier for holes (ϕ_p) is increased for FE2 and reduced for FE1.

ferroelectric polarization normal to the interfaces is more stable with smaller lattice parameters. In the case of TiO_2-terminated PTO layers, SRO/PTO interfaces strongly suppress the ferroelectric polarization in PTO, requiring very small lattice parameters for the ferroelectric state to become stable. It was demonstrated that the influence of SRO/PTO interfaces on the ferroelectric stability is longer ranged compared to Pt/PTO interfaces. The asymmetric combination of electrodes (Pt and SRO) enhances the ferroelectric polarization pointing from SRO to Pt while the opposite polarization becomes less stable.

As the lattice parameter increases, the rumpling of PTO atomic layers due do spontaneous polarization decreases and the difference of those between PbO and TiO_2 layers becomes reduced. For $m=4$, the PTO layer rumpling in Pt/PTO/SRO asymmetric capacitors is similar to that in the symmetric ones (Pt/PTO/Pt and SRO/PTO/SRO).

For the symmetric capacitors, it is expected that the lattice parameter will not strongly affect the Schottky barrier height. The influence of ferroelectric polarization on the Schottky barrier is larger in SRO/PTO/SRO than in Pt/PTO/Pt. The contribution of the electrical field generated by the asymmetric electrodes influences the Schottky barriers significantly. The switch from FE1 to FE2 of the PTO polarization in the Pt/PTO/SRO capacitor changes the Schottky barriers of the SRO electrode by about 1.0 eV.

ACKNOWLEDGMENTS

J.-M.A. and C.E. acknowledge financial support from the German Research Foundation (Project No. El 155/17-2 in the DFG priority program 1157 "Integrated electroceramic functional structures," and Project No. El 155/22-1), and from the European Commission [Contract No. NMP3-CT-2005-013862 (INCEMS)]. J.-M.A. and C.E. thank Matous Mrovec for valuable discussions.

[1] J. Junquera and P. Ghosez, Nature (London) **422**, 506 (2003).
[2] N. Sai, A. M. Kolpak, and A. M. Rappe, Phys. Rev. B **72**, 020101(R) (2005); **74**, 059901(E) (2006).
[3] Y. Umeno, B. Meyer, C. Elsässer, and P. Gumbsch, Phys. Rev. B **74**, 060101(R) (2006).
[4] C.-G. Duan, R. F. Sabirianov, W.-N. Mei, S. S. Jaswal, and E. T. Tsymbal, Nano Lett. **6**, 483 (2006).
[5] M. Stengel, D. Vanderbilt, and N. Spaldin, Nat. Mater. **8**, 392 (2009).
[6] G. Gerra, A. K. Tagantsev, and N. Setter, Phys. Rev. Lett. **98**, 207601 (2007).
[7] B. Meyer, K. Hummler, C. Elsässer, and M. Fähnle, J. Phys.: Condens. Matter **7**, 9201 (1995).
[8] F. Lechermann, F. Welsch, C. Elsässer, C. Ederer, M. Fähnle, J. M. Sanchez, and B. Meyer, Phys. Rev. B **65**, 132104 (2002).
[9] D. Vanderbilt, Phys. Rev. B **32**, 8412 (1985).
[10] C. Elsässer, N. Takeuchi, K. M. Ho, C. T. Chan, P. Braun, and M. Fähnle, J. Phys.: Condens. Matter **2**, 4371 (1990).
[11] K. M. Ho, C. Elsässer, C. T. Chan, and M. Fähnle, J. Phys.: Condens. Matter **4**, 5189 (1992).
[12] C. Elsässer, K. M. Ho, C. T. Chan, and M. Fähnle, J. Phys.: Condens. Matter **4**, 5207 (1992).
[13] T. Ochs and C. Elsässer, Z. Metallk. **93**, 406 (2002).
[14] J. M. Albina, M. Mrovec, B. Meyer, and C. Elsässer, Phys. Rev. B **76**, 165103 (2007).
[15] M. Mrovec, J. M. Albina, B. Meyer, and C. Elsässer, Phys. Rev. B **79**, 245121 (2009).
[16] H. J. Monkhorst and J. D. Pack, Phys. Rev. B **13**, 5188 (1976).
[17] C. L. Fu and K. M. Ho, Phys. Rev. B **28**, 5480 (1983).
[18] D. Vanderbilt, Phys. Rev. B **41**, 7892 (1990).
[19] P. E. Blöchl, Phys. Rev. B **50**, 17953 (1994).
[20] G. Kresse and J. Hafner, Phys. Rev. B **47**, 558 (1993).
[21] G. Kresse and J. Furthmüller, Phys. Rev. B **54**, 11169 (1996).
[22] A. M. Kolpak, N. Sai, and A. M. Rappe, Phys. Rev. B **74**, 054112 (2006).
[23] A. Baldereschi, S. Baroni, and R. Resta, Phys. Rev. Lett. **61**, 734 (1988).
[24] L. Colombo, R. Resta, and S. Baroni, Phys. Rev. B **44**, 5572 (1991).
[25] J. Junquera, M. Cohen, and K. Rabe, J. Phys.: Condens. Matter **19**, 213203 (2007).
[26] G. Henkelman and H. Jónsson, J. Chem. Phys. **113**, 9978 (2000).
[27] X. Gu, N. Izyumskaya, V. Avrutin, H. Morkoç, T. Kang, and H. Lee, Appl. Phys. Lett. **89**, 122912 (2006).
[28] S. Picozzi, G. Profeta, A. Continenza, S. Massidda, and A. J. Freeman, Phys. Rev. B **65**, 165316 (2002).
[29] J. Goniakowski and C. Noguera, Interface Sci. **12**, 93 (2004).
[30] B. Meyer and D. Vanderbilt, Phys. Rev. B **63**, 205426 (2001).